ISSN 0022-4766, Journal of Structural Chemistry, 2019, Vol. 60, No. 5, pp. 713-726. © Pleiades Publishing, Inc., 2019.
Text © The Author(s), 2019, published in Zhurnal Strukturnoi Khimii, 2019, Vol. 60, No. 5, pp. 748-760.

A COMPARISON OF NH_5^{2+} AND CH_5^+ IONS AND DEUTERATED VARIANTS OF $NH_xD_{(5-x)}^{2+}$: REAL OR ARTEFACTUAL ROTATION?

M. Monajjemi

Protonated NH_5^{2+} has unusual vibrational and rotational behavior because its three nonequivalent equilibrium structures have nearly identical energies and its five protons scramble freely, while in the CH_5^+ structure, five hydrogen atoms are bonded to the carbon atom by sharing eight valence electrons. Although a few theoretical papers have been published on quantum mechanics of those systems. Better understanding requires spectral and conformational analyses. CASSCF (8, 9) calculations with the correlation consistent polarized valence double and triple zeta basis sets are accomplished for estimating the vibrational data and zero-point energies of those two ions. The present results indicate that normal modes agree qualitatively with $NH_xD_{(5-x)}^{2+}$ and one of the normal modes indicates that NH_5^{2+} is highly fluxional and has a complex spectrum while the broken N–H bonds are reformed all the time. The spectrum of mode 10 is highly complex with red and some blue shifts. In particular, modes 6 and 12 are attributed to the rapid coupling of the N–H stretching normal mode to motions more closely related to isomerization, i.e., bending or rocking. There have been long debates whether NH_5^{2+} has a structure at all or not and if the rotation is real or artefactual.

DOI: 10.1134/S0022476619050032

Keywords: quantum rotation, NH_5^{2+} ion, CH_5^+ ion, deuterated variants.

INTRODUCTION

The investigation of the quantum rotational dynamics of a molecular system might provide important data on the mechanical structures and forces between atoms in molecules (AIM) and also among the molecular constituents within a single molecule (non-bonded interaction). In this study, protonated NH_5^{2+} and CH_5^+ ions with the three-center two-electron bonding have been a subject of various theoretical and experimental investigations since their first detection in 1952 [1-7]. It is an important intermediate in hypercoordination chemistry and superacid [8, 9] and is highly relevant in the fields such as plasma chemistry [10-12]. For decades and even up to now, NH_5^{2+} and CH_5^+ have provided some challenges for

Department of Chemical Engineering, Central Tehran Branch, Islamic Azad University, Tehran, Iran; Maj.monajjemi@iauctb.ac.ir. Original article submitted May 14, 2018; revised June 28, 2018; accepted July 02, 2018.

theoreticians and as well as experimentalists due to the correlated large-amplitude motion of their five protons around the carbon atom.

In 2004, Keiranand coworkers [13] have applied aquantum diffusion Monte-Carlo calculation for estimating ground-state zero-point energies (ZPEs) from interpolated PES. It has been exhibited that ZPE as a function of the number by 150 points has converged to within ±0.5 kJ/mol [13] for CH_5^+. And also converged fully anharmonic ZPE on interpolated PES calculated as 132.72 kJ/mol was significantly lower than the CCSD(T)/aug-cc-pVTZ or MP2/cc-pVTZharmonic ZPE of the global minimum structure (C_s), which were found to be 134.75 kJ/mol and 136.7 kJ/mol respectively [5]. Up to now there is no attempt to compare the structures of CH_5^+ and NH_5^{2+} ions by rotational and conformational analyses.

Based on the behavior and bimodality of the H–H radial distribution function, it is obvious that the ground state of NH_5^{2+} and CH_5^+ wave function does have a global minimum energy configuration of the C_s character. However, there is considerable delocalization of some protons and the calculated rotational constants proposed by Brown [6] (for both C–H and N–H bonds), showing a ground state structure with a symmetrical structure rather than the C_s configuration. NH_5^{2+} consists of three configurations [14], including static equilibrium structures of the ground state and two transition states, which mainly determine the dynamics of NH_5^{2+}. Those are: (1) e-C_s (I) isomer consists of a three-center two-electron bond associating two hydrogen atoms in addition to a NH_3 tripod, while the H_2 moiety is attached in the eclipsed orientation; (2) staggered (s-C_s) saddle point [15] obtained by 30° rotation of the H_2 moiety is barely higher in energy [16] than the ground state position; (3) third stationary point is a saddle point [14, 15] with the C_{2v} symmetry. The approach enables an easy exchange of hydrogen sites, the so-called hydrogen scrambling [14]. This phenomenon occurs by isomerization transitions between different degenerate states of e-C_s through the s-C_s transition and the C_{2v} structure [14, 17].

It might be understood from ZPE of the harmonic data which differ by about 100 cm^{-1} in the first location of the D atom. According to the calculations of McCoy et al. [3], the lowest energies of the C_s (I) configurations were obtained for an arrangement in which three deuterons are placed in the tripod section. Schreiner et al. calculated harmonic ZPE of those species for e-C_s (I), s-C_s (II), and C_{2v} structures with 136.8 kJ/mol, 136.4 kJ/mol, and 132.0 kJ/mol respectively and scaled its harmonic frequency by 0.95 for estimating anharmonic effects [14]. It has been exhibited by this work that all five hydrogen atoms possess identical N–H and H–H radial distribution functions within the nuclear vibrational wave function. There is substantial proton scrambling even at 0 K, and this is an uncertain result.

Although those values are the best data in comparison with the infrared spectra of N–H and C–H bonds, Keiran [13] obtained a reasonable value of harmonic ZPE at the 0.985 point on CCSD (T)/aug′-cc-pVTZ interpolated PES.

Obviously, both CH_5^+ and NH_5^{2+} ions are quasi-rigid molecules with a well-described molecular structure. However, for its protonation a thorough discussion of the electronic structures is needed. This can be related to its abnormal flat potential energies, which provides complications. Large-magnitude motion for taking place, which is a reason for fluxionality, persists even at a very low temperature (≠0 K) due to quantum-mechanical fluctuation (QMF) treatment of the highly correlated scrambling motion of the five protons [17].

In 2010, through the deuterated variants of CH_5^+, Ivanov [18] and coworkers revealed that, in stark contrast to the traditional approach, the isotopologue spectra of $NH_xD_{(5-x)}^{2+}$ (x = 0, 1, … 5), recorded in an ion trap using the laser-induced reaction [17] technique [18] bear almost no resemblance to one another [19, 20]. The SCF simulation represents all six vastly different IR spectra and allows the assignment of their aspects [21]. The analysis exactly confirms that the spectra observed for x = 1, 2, 3 H and D site occupations are confused but for x = 4 the combinatorial symmetry is broken for these atoms due to QMF within the fluxional molecular frame. There have been a few polemical discussions of the experiments which indicate that the deuteron transfer from ND_5^{2+} to NH_5^{2+} can create stable isotopomers [22].

Via an important procedure, D–H exchange reactions results in isotope enrichment at low temperatures [5]. In 2004, *via* QDMC Brown [6] reported ZPEs for CD_5^+ and CH_5^+ as 8080 cm^{-1} and 10975 cm^{-1}, respectively [6]. Due to the C_s(I) structure described above, the $CD_3H_2^+$ isotopomer is of specific interest.

Although through the hydrogen scrambling approach some complexity has been cleared for the quantum ground state of the NH_5^{2+} structure, hydrogen scrambling is not the root of all the known intricacies [17, 18]. In particular, it has been discussed in these studies that NH_5^{2+} undergoes hydrogen scrambling even in the quantum ground state and that the resulting correlated pseudo-rotational dynamics is due to symmetry breaking consisting of several small barriers for $NH_xD_{(5-x)}^{2+}$variants.

THEORETICAL

Electron densities have been described as [23-25]

$$\rho(r) = \eta_i \,|\, \varphi_i(r) \,|^2 = \sum_i \eta_i \,|\sum_l C_{l,i}\chi_i(r)\,|^2 \tag{1}$$

and η_i, φ_i, and $\chi_i(r)$ are occupation numbers of orbitals (i), orbital wave functions $\chi_i(r)$, and basic functions respectively. In addition, $C_{l,i}$ are matrix coefficients, therefore electron densities can be explicitly defined as e/Bohr^3 [23-25]:

$$\nabla\rho(r) = \left[\left(\frac{\partial\rho(r)}{\partial(x)}\right)^2 + \left(\frac{\partial\rho(r)}{\partial(y)}\right)^2 + \left(\frac{\partial\rho(r)}{\partial(z)}\right)^2\right]^{1/2}, \tag{2}$$

$$\nabla\rho(r) = \frac{\partial^2\rho(r)}{\partial x^2} + \frac{\partial^2\rho(r)}{\partial y^2} + \frac{\partial^2\rho(r)}{\partial z^2}. \tag{3}$$

The (–) and (+) values of this function correspond to locally concentrated and locally depleted respectively. The electrons localizations have been built by Bader′s studies [26]. We have calculated densities of hydrogen and deuterium atoms in deuterated variants of $NH_xD_{(5-x)}^{2+}$ *via* a relationship between $\nabla^2\rho$ and valence shell repulsion [26]. Kinetic energies $K(\boldsymbol{r})$ cannot be defined individually, since the expected values of this operator [25] $\langle\varphi|-(1/2)\nabla^2|\varphi\rangle$ can be reproduced by integrating through an alternative definition. One of the most used explications can be extended as [23-25]:

$$K(\mathbf{r}) = -\frac{1}{2}\sum_i \eta_i\varphi_i^*(r)\nabla^2\varphi_i(r). \tag{4}$$

The Lagrangian kinetic densities $G(\mathbf{r})$ are also mentioned as a positive definition as follows:

$$G(\mathbf{r}) = -\frac{1}{2}\sum_i \eta_i \,|\, \nabla\varphi_i \,|^2 = \frac{1}{2}\sum_i \eta_i \left\{\left[\left(\frac{\partial\varphi_i(r)}{\partial(x)}\right)^2 + \left(\frac{\partial\varphi_i(r)}{\partial(y)}\right)^2 + \left(\frac{\partial\varphi_i(r)}{\partial(z)}\right)^2\right]\right\}. \tag{5}$$

$G(\mathbf{r})$ and $K(\mathbf{r})$ are directly related by Laplacian of the densities

$$\frac{1}{4}\nabla^2\rho(r) = G(\mathbf{r}) - K(\mathbf{r}). \tag{6}$$

Based on kinetic energies, ground-state ZPEs can be evaluated as a function of the distinct number (by about 150 points), which converged within ±0.5 kJ/mol [13].

According to transition state energies, the frequency of a hydrogen atom moving to a radial distribution function can be expressed as:

$$\Gamma = \vartheta * \exp\left(-\frac{\Delta E_h}{K_B T}\right), \tag{7}$$

where ΔE_h is the difference between the energies and ϑ^*, are the effective vibrational frequencies. In this work, the harmonic approximation of isotope bonding vibration on the uncoupled situation is attained through rescaling the frequency using the reduced mass ratio $\omega_D = \omega_H \sqrt{\frac{\mu_H}{\mu_D}}$ from the respective eigen-frequency $\omega_X = \omega_H \sqrt{\frac{K_X}{\mu_X}}$.

Beck and Edgecombe obtained the spin probability correlation with Fermi holes through a novel electron localization function (ELF) [27]

$$\mathrm{ELF}(r) = \frac{1}{1 + (D(r) / D_0(r))^2}, \tag{8}$$

where

$$D(r) = \frac{1}{2}\sum_i \eta_i \,|\nabla\varphi_i|^2 - \frac{1}{8}\left[\frac{||\nabla\rho_\alpha|^2}{\rho_\alpha(r)} + \frac{||\nabla\rho_\beta|^2}{\beta(r)}\right] \tag{9}$$

since

$$\rho_\alpha(r) = \rho_\beta(r) = \frac{1}{2}\rho, \tag{10}$$

D and D_0 terms can be simplified as

$$D(r) = \frac{1}{2}\sum_i \eta_i \,|\nabla\varphi_i|^2 - \frac{1}{8}\left[\frac{|\nabla\rho|^2}{\rho_\alpha(r)}\right], \tag{11}$$

$$D_0(r) = \frac{3}{10}(3\pi^2)^{2/3}\rho(r)^{5/3}. \tag{12}$$

Also for a close-shell system equation (9) can be rewriten as:

$$D_0(r) = \frac{3}{10}(6\pi^2)^{2/3}[\rho_\alpha(r)^{5/3} + \rho_\beta(r)^{5/3}]. \tag{13}$$

Savin et al. have reinterpreted [28] ELF in view of kinetic energies, which makes ELF also useful for Kohn–Sham wave-functions in DFT methods. Tsirelson [29] and Stash showed that $D(\boldsymbol{r})$ reveals excess kinetic densities under the Pauli repulsion rules, while $D_0(\boldsymbol{r})$ can be considered as Thomas–Fermi densities.

Localized orbital locators (LOL) were defined by Schmider [30] and Becke as another novel function for locating in the high regions as the same ELF.

$$\mathrm{LOL}(r) = \frac{\tau(r)}{1 + \tau(r)} \tag{14}$$

and

$$(r) = \frac{D_0(r)}{\frac{1}{2}\sum_i \eta_i \,|\nabla\varphi_i|^2}. \tag{15}$$

By this study the ELF and LOL parameters of hydrogen and deuterium atoms in deuterated variants of $NH_xD_{(5-x)}^{2+}$ have been calculated to reveal the situation and position of five proton scrambling and their mechanism as artefactual rotation. In addition, a few years ago Aslangul and coworkers attempted to decompose diatomic and triatomic molecules into reciprocal monopolized spaces by minimizing information entropies [31]. Parr et al. [32] have discussed the relationship between the information entropies and molecular similarities, which has been exhibited by the formula of Shannon′s information entropies as follows [33]:

$$S = -\int P(x)\ln P(x)dx. \tag{16}$$

The electrostatic potentials (ESP) measure the electrostatic interaction among the unit point charges placed at *r* and the systems. A positive (negative) value implies that the current position is dominated by nuclear (electronic) charges.

ESP has been widely used for prediction in statistical analysis. Murray and his coworkers [34] found the set of functions called GIPF that relates ESP in a molecular system and physical properties.

COMPUTATIONAL METHODS

Calculations were performed using GAMESS-US packages [35] and the Gaussian software. There are various situations of hydrogen and deuterium position interactions in $NH_xD_{(5-x)}^{2+}$ systems. Using the extensive direct dynamics of the potential and the gradient, first PES and dipole moment have been calculated at the CASSCF level of theory with cc-pVDZ and cc-pVTZ basis sets [36].

In this study, full dimensional *ab initio* based PES and *ab initio* electron energy gradients are obtained through calculations using post-HF, Møller–Plesset, and DFT theories with the correlation consistent polarized valence double and triple zeta basis sets.

Switching to energies, the most accurate calculations of binding energies and scrambling barriers are considered to be obtained by CCSD(T) and CASSCF methods. Although a normal basis set (aug-cc-pVTZ) has been used in the CCSD(T) calculations, the result for the scrambling barrier in various NX_5^+ is close to the values reported by Müller et al. [16]. CCSD (T) also yields rotational energies in good agreement with MP2 but underestimates the scrambling barrier. It would be too expensive to use both of them, and therefore, a cheaper method, i.e. DFT, has to be considered. Through redundant internal coordinates, several PESs in few internuclear distances were fitted to these data. The potential energies and gradient data for each atom of $NH_xD_{(5-x)}^{2+}$ generated an analytical multinomial expression, using Multiwfn analyzing software [23-25] as variables in the complete set of inverse internuclear distances.

In this work, we have also focused on getting the optimized results from advanced DFT methods, including m06 and m06-L. M062x, m06-L, and m06–HF are a novel meta-hybrid DFT functional with good correspondence [37] and are useful for calculating energies of the distance between atoms in $NH_xD_{(5-x)}^{2+}$. The m06 and m06-L (DFT) functional is based on an iterative solution of the Kohn–Sham equation [38] in a plane-wave set with the projector-augmented wave pseudo-potentials. The Perdew–Burke–Ernzerhof [39] (PBE) exchange-correlation (XC) functional of the generalized gradient approximation (GGA) is adopted. Based on our previous works [40-53] concerning the approaches of ELF, LOL and density quantum energies, we strive to discuss a useful method to understand more about $NH_xD_{(5-x)}^{2+}$ treatments.

RESULTS AND DISCUSSION

Obviously, the simplest type of rigid rotors are those that have a single rotational degree of freedom, such as ammonia compounds consisting of ammonia groups (NH_3) or methyl halides containing CH_3. In those rigid molecular compounds, the ammonia groups can rotate around a fixed molecular axis under an external field hindering rotation, thus representing several different rotations. The optimization and ZPE determination of $NH_xD_{(5-x)}^{2+}$ was performed as well as for those compounds with the reaction as follows: $NH_5^{2+} \rightarrow NH_3^{2+} + H_2$, $NHD_4^{2+} \rightarrow ND_3^{+} + HD$, $NH_2D_3^{2+} \rightarrow ND_3^{+} + H_2$, $NH_3D_2^{2+} \rightarrow NH_3^{2+} + H_2$, $NH_4D^{2+} \rightarrow NH_2D^{2+} + HD$ and $ND_5^{2+} \rightarrow ND_3^{2+} + D_2$.

The data on density energies, charges from ESP, electrostatic potential, ionization energy, ellipticity of electron densities, Eta index and some other physical properties for carbon, nitrogen, deuterium, and hydrogen atoms are listed in Tables 1-5 and Figs. 1-9.

TABLE 1. Various Energy Densities, ELF, LOL, and Local Information Entropy for ND_5^{2+} *via* ccsd(T)/AUG-cc-pvdz

Atoms	D–N bond length	Electron density	ESP (10^2)	Kinetic energy density [$G(\boldsymbol{r})$]	Hamiltonian energy density [$K(\boldsymbol{r})$]	Potential energy density [$U(\boldsymbol{r})$]	Electron localization function (ELF)	Local information entropy	Ellipticity of electron density	Eta index	Localized orbital locator (LOL)
N(1)	–	0.191	–0.200	0.182	0.241	–0.241	0.999	–0.564	0.000	–1.00	0.998
D(2)	1.11	0.268	–0.479	0.183	0.313	–0.315	0.999	0.972	0.001	–1.10	0.949
D(3)	1.11	0.268	–0.479	0.183	0.313	–0.315	0.997	0.973	0.001	–1.10	0.946
D(4)	1.11	0.268	–0.477	0.184	0.314	–0.316	0.998	0.971	0.002	–1.11	0.947
D(5)	1.11	0.267	–0.474	0.181	0.312	–0.315	0.997	0.977	0.024	–1.09	0.946
D(6)	1.06	0.323	–0.466	0.265	0.367	–0.369	0.999	0.110	0.035	–1.12	0.957

TABLE 2. Various Energy Densities, ELF, LOL, and Local Information Entropy for CH_5^+ with CASSCF(8, 9)/cc-pvdz Quantum Calculations

Atoms	C–H bond length	Electron density	Kinetic energy density [$G(\boldsymbol{r})$]	Hamiltonian energy density [$K(\boldsymbol{r})$]	Potential energy density [$U(\boldsymbol{r})$]	Electron localization function (ELF)	Local information entropy	Ellipticity of electron density	Eta index	Localized orbital locator (LOL)
H(2)	1.10	0.346	0.242	0.293	–0.295	0.99	0.116	0.001	–1.10	0.953
H(3)	1.10	0.346	0.242	0.293	–0.295	0.99	0.116	0.001	–1.10	0.953
H(5)	1.12	0.335	0.235	0.288	–0.290	0.99	0.113	0.001	–1.10	0.952
H(4)	1.24	0.300	0.238	0.260	–0.263	0.99	0.105	0.028	–1.09	0.942
H(6)	1.24	0.292	0.255	0.253	–0.255	0.99	0.103	0.035	–1.09	0.935

TABLE 3. ESP, Various Energy Densities, LOL, ELF, and Local Information Entropy for H Atoms in $CH_xD^+_{(5-x)}$ Variants

Hydrogen properties in $CH_xD^+_{(5-x)}$	ESP (10^2)	Kinetic energy density [$G(\boldsymbol{r})$]	Hamiltonian energy density [$K(\boldsymbol{r})$]	Potential energy density [$U(\boldsymbol{r})$]	Electron localization function (ELF)	Local information entropy	Ellipticity of electron density	Eta index	Localized orbital locator (LOL)
CHD_4^+: x = H(6)	–0.466	0.279	0.248	–0.251	0.99	0.102	0.035	–1.09	0.93
$CH_2D_3^+$: x = H(6)	–0.466	0.280	0.249	–0.252	0.99	0.102	0.036	–1.09	0.93
$CH_2D_3^+$: x = H(4)	–0.464	0.256	0.256	–0.259	0.99	0.104	0.026	–1.09	0.94
$CH_3D_2^+$: x = H(4)	–0.464	0.256	0.256	–0.259	0.99	0.104	0.025	–1.09	0.94
$CH_3D_2^+$: x = H(5)	–0.477	0.252	0.282	–0.285	0.99	0.113	0.002	–1.10	0.95
CH_4D^+: x = H(2)	–0.464	0.256	0.256	–0.259	0.99	0.104	0.025	–1.09	0.94
CH_4D^+: x = H(3)	–0.477	0.252	0.282	–0.285	0.99	0.113	0.002	–1.10	0.95
CH_5^+: x = H(4)	–0.459	0.238	0.260	–0.263	0.99	0.105	0.028	–1.09	0.942
CH_5^+: x = H(6)	–0.460	0.255	0.253	–0.255	0.99	0.103	0.035	–1.09	0.935

Fitted PES is tested by comparing it against additional electron energy calculations and normal mode frequencies at the three lowest stationary points obtained from the fitting against *ab initio* ones. Rotational constants along the N–X and H–X bond lengths and the tunneling coordinates *via* ELF, LOL, energy densities, local information entropy, geometry optimization of $NH_xD^{2+}_{(5-x)}$ variants (x varies from 0 to 5), and related normal modes have been calculated and are presented

in Table 5 and Fig. 8. In addition, they were compared with the corresponding harmonic oscillator and standard classical molecular dynamics data (Fig. 7 and Tables 4, 5). The wave function delocalization is analyzed through the Multiwfn software by comparing the NX_5^{2+} (X = H and D) distributions with those obtained when all hydrogen atoms were replaced by deuterium ones (Table 3).

ELF has been calculated *via* equation (8) for all ions, and the data are listed in Tables 1-3; LOL has been made through equations (14), (15) for those items. The densities for open and closed-shell systems have been estimated *via* equations (9)-(13). The spin density from the difference between α and β densities can be calculated through the expression $\rho^s(r) = \rho^\alpha(r) - \rho^\beta(r)$, then the spin polarization parameter function was returned instead of the spin density $\xi(r) = \dfrac{\rho^\alpha(r) - \rho^\beta(r)}{\rho^\alpha(r) + \rho^\beta(r)}$. The situation with LOL for NH_5^{2+} from the CASSCF {(8,9)/cc-pvdz calculation} has been shown in Fig. 3.

Since, in the Born–Oppenheimer approximation the molecular wave function can be disjointed as $\Psi_{mol} = \Psi_{trans}\Psi_{el}\Psi_{vib}\Psi_{rolt}\Psi_{ns}$, so, in order to induce quantum rotation of the NH_3 group, a change in the nuclear spin state must occur. Therefore, if electrons are completely localized, then they can be distinguished from those outside. Bader [26] found that the areas which had large electron localization might have large magnitudes of Fermi hole integration. Although $D_0(\mathbf{r})$ from equations (12) and (13) is introduced into ELF as the reference. ELF reveals basically a relative localization (ELF is within the range [0, 1]). A large ELF value means that electrons are extremely localized, which indicates that there are covalent bonds in the regions. Based on ELF variables (as can be seen in Tables 1-4), all X–N bond strengths are equal to strong covalent bonds. As a result, the disassociation mechanism of the $NH_xD_{(5-x)}^{2+}$ to produce H_2 or D_2 seems bizarre but is true. Ivanov [18] and coworkers have discussed it through assigning the spectra of the isotopologues with experimental and computed IR spectra of NH_5^{2+} and all its H/D isotopologues (including mass-rescaled ND_5^{2+} and NH_5^{2+}) with the simulated spectra to a particular mode (except for bends). Based on full decomposition intoisotopomer contributions, they exhibited subsequent spectral occupation probabilities for the disentan- gling proton in the moiety where upper/lower bars indicate the quantum/classical distributions. As shown in Figs. 4, 6, it is believed that within classical mechanics, the five different sites in NX_5^{2+} are expected to be populated by H or D for all categories of $NH_xD_{(5-x)}^{2+}$.

Based on our results (Tables 3-5 and Figs. 6, 7), it is supposed that only two N–X bonds in a part of molecules exhibit properly quantum effects on the nuclei (as quantum particles through the high rotation) while the other parts of the molecules have classical particle behavior (lower rotation) which is the so-called artefactual rotation. ELF has been widely used for a wide variety of systems, such as these kinds of small molecules, to reveal the atomic shell structure and the

TABLE 4. ESP, Various Energy Densities, LOL, ELF, and Information Entropy for N Atoms of $NH_xD_{(5-x)}^{2+}$ Variants

Carbon properties in $CH_xD_{(5-x)}^{+}$	ESP (10^2)	Kinetic energy density [$G(\mathbf{r})$]	Hamiltonian energy density [$K(\mathbf{r})$]	Potential energy density [$U(\mathbf{r})$]	Electron localization function (ELF)	Local information entropy	Ellipticity of electron density	Eta index	Localized orbital locator (LOL)
NH_5^{2+}	–0.200	0.182	0.241	–0.241	0.999	–0.564	0.000	–1.00	0.998
ND_5^{2+}	–0.198	0.179	0.240	–0.239	0.998	–0.563	0.000	–1.02	0.999
NHD_4^{2+}	–0.199	0.180	0.240	–0.240	0.998	–0.563	0.000	–1.01	0.997
$NH_2D_3^{+}$	–0.198	0.181	0.241	–0.241	0.998	–0.562	0.000	–1.02	0.997
$NH_3D_2^{2+}$	–0.199	0.180	0.240	–0.240	0.999	–0.565	0.000	–1.04	0.996
NH_4D^{2+}	–0.198	0.179	0.239	–0.239	0.997	–0.560	0.000	–1.05	0.995

TABLE 5. Rotational Temperatures, Rotational Constants, Zero-Point Vibrational Energy, and Thermal Energy for $NH_xD^{2+}_{(5-x)}$ Variants

$CH_xD^{+}_{(5-x)}$	Rotational temperatures				Rotational constants (GHZ)			Zero-point vibrational energy, kcal/mol	*E* (thermal), kcal/mol
	x	*y*	*z*	total	*x*	*y*	*z*		
NH_5^{2+}					162.90	162.90	120.02		
CD_5^+	3.135	2.749	2.607	4.92	65.327	57.293	54.339	23.643	25.997
CHD_4^+	3.345	3.013	3.010	5.42	69.699	62.781	62.737	25.244	27.538
$CH_2D_3^+$	3.886	3.625	3.147	6.18	80.982	75.540	65.581	27.063	29.318
$CH_3D_2^+$	4.496	4.151	3.562	7.09	93.693	86.494	74.237	28.620	30.825
CH_4D^+	5.480	4.554	4.227	8.29	114.199	94.906	88.081	30.528	32.705
CH_5^+	6.258	4.818	4.562	9.11	130.40	100.392	95.05	31.744	33.811

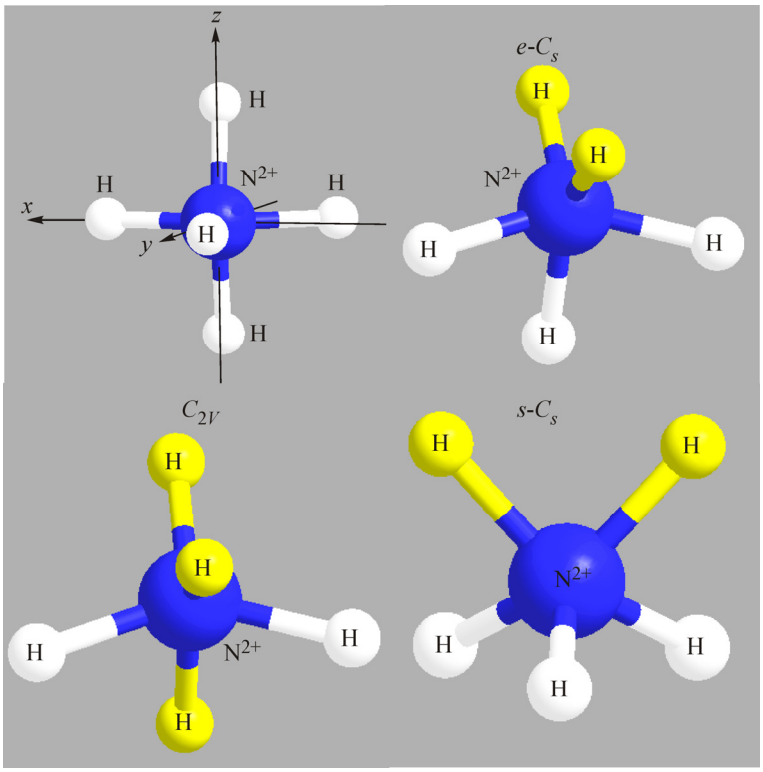

Fig. 1. Eclipsed (e-C_s for global minima) structures with the NH_3 tripod (white and dark), staggered saddle point (s-C_s for TS for the H_2 rotation) and H_2 moiety (grey); saddle point structure (C_{2v} for H_2–NH_3 proton exchange) with three coplanar hydrogen atoms (grey).

classification of chemical bonding to verify charge-shift bonds. This approach, which has a similar expression compared to ELF, became stronger *via* the LOL data. Jacobsen [54] pointed out that LOL conveys a more decisive and clearer picture than ELF. Obviously, LOL can be interpreted in kinetic energy in the same way as for ELF. However, LOL can also be interpreted in view of localized orbitals. Small (large) LOL values usually appear in the boundary (inner) area of localized orbitals because the gradient of the orbital wave-function is large (small) in this area. The LOL value range is identical to ELF, namely [0, 1]. As can be seen in Tables 1 and 2, the LOL values are different for two levels of classical occupations and quantum populations.

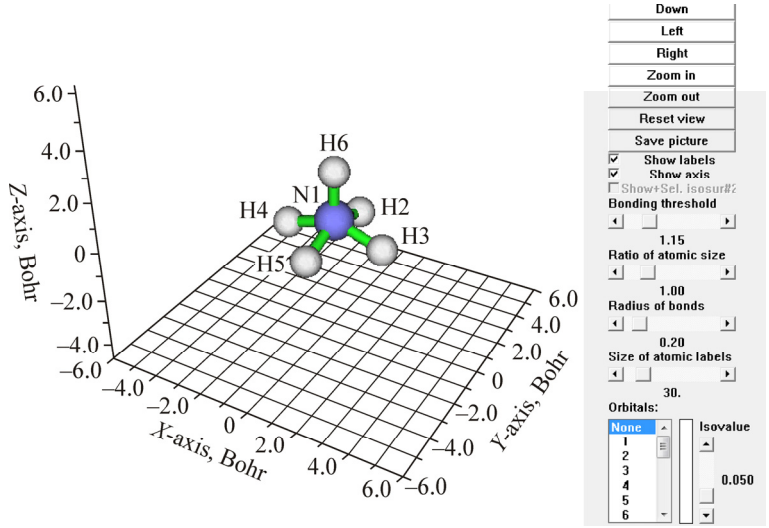

Fig. 2. H(6) and H(4) hydrogen atoms prefer to be out of the NX_3 tripod based on quantum approaches.

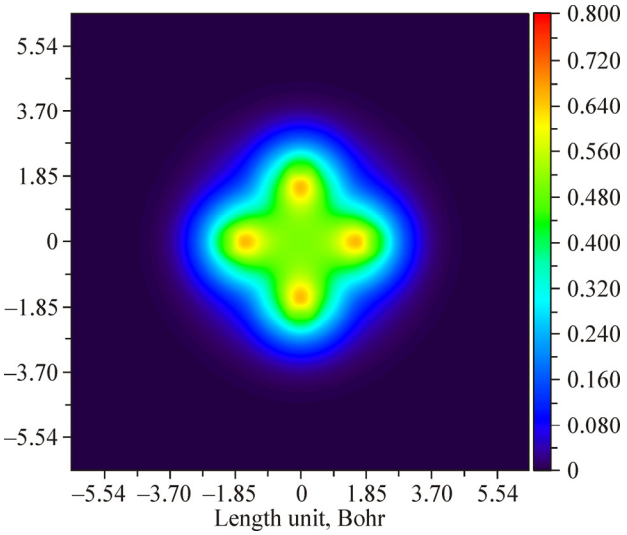

Fig. 3. LOL calculation and color-filled map of NH_5^{2+} through Casscf(8,9)/cc-pvdz calculation.

Normal mode analysis based on quantum approaches reveals that protons prefer to accumulate in the X_2 moiety for all mixed isotopologues whereas deuterons prefer to be in the NX_3 tripod (Tables 5-7 and Figs. 7-9). Average local ionizations for separated fragments (Fig. 6) indicate that the energy separation is a function of the HD situation, which are equal for $NH_4D^{2+} \rightarrow NH_2D^{2+} + HD$ and $NHD_4^{2+} \rightarrow CD_3^+ + HD$ and different for $NH_5^+ \rightarrow NH_3^+ + H_2$ and $ND_5^+ \rightarrow ND_3^+ + D_2$. The N(1)–H(6) stretching band as the lowest frequency has been associated with the relative motion of the H_2 moiety with respect to the methyl tripod in protonated methane, which indicates that NH_5^{2+} is actually composed of two subunits NX_3 and X_2 in hydrogen scrambling. Thus, the results indicate that H atoms freely exchange by passing over the isomerization barriers between C_{2v} and C_s energy levels. The neutralization of protonated methane by opposite rearranging with free electrons is one of the important approaches for this study.

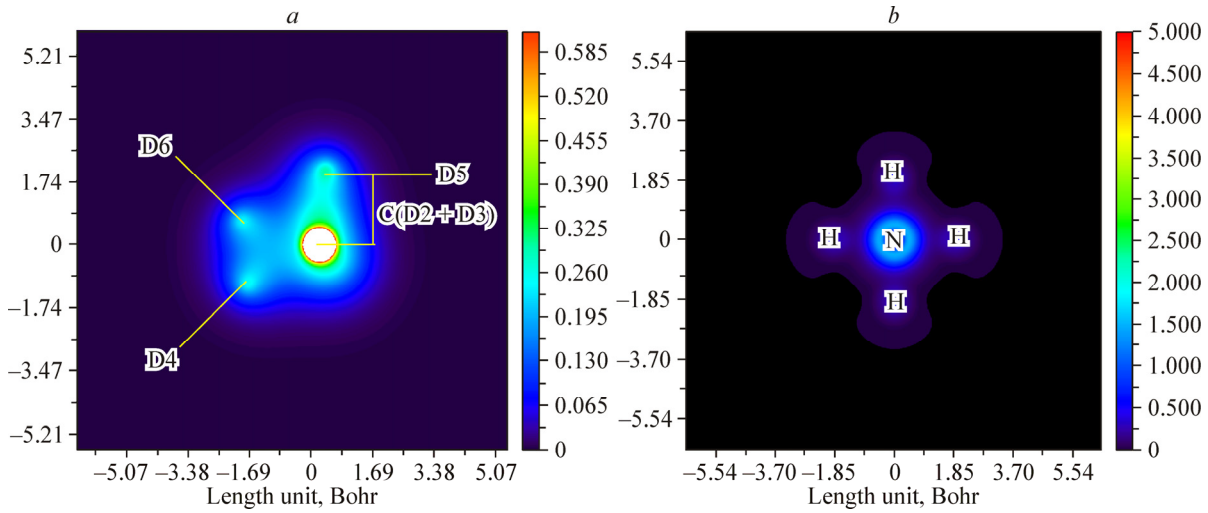

Fig. 4. Electron density color-field map for $D_5 \rightarrow D_3 + D_2$ (note: the D6, D5, D4 are atom numbers for three deuterium while the atom number of Carbon is C1) (*a*) and NH_5^{2+} configuration (*b*). Note the fifth hydrogen atom behind the molecule.

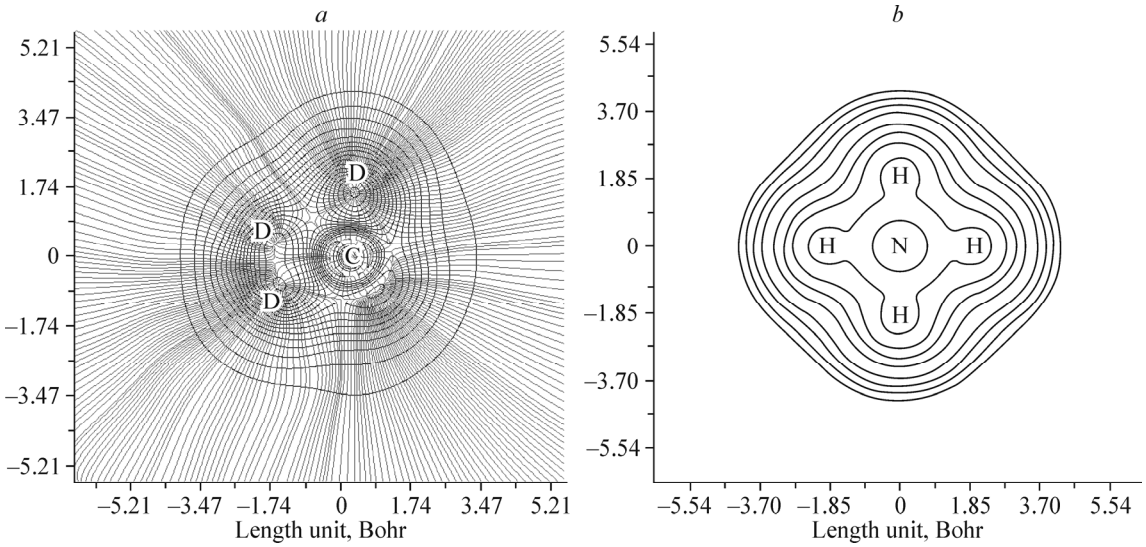

Fig. 5. LOL gradient map of CD_5^+ (*a*) and NH_5^+ (*b*) in quantum rotation.

The energy level diagram (Fig. 6 and Table 5) shows the two energetically accessible dissociation limits of NH_5^{2+} which is formed with C_s on the neutral surface. The three-body dissociation limit is nearly resonant with the 3*s* Rydberg state. The results of the electron density ellipticity from Tables 1-4 are described using the correct "fluxional" phase-space sampling of NH_5^{2+} which are vertical, resonant, and non-resonant in good correspondence with the experimental data.

In Fig. 6 the shoulder near 1.714 Bohr corresponds to the D_2 moiety, whereas the peak at 2.114 Bohr corresponds to H–D groups. Moreover, the shoulder near 2.5 Bohr corresponds to the H_2 moiety. It is clear that most of the energy goes into internal excitation (vibrational and rotational) of NH_3^{2+}+H_2. This channel exhibits a bimodal distribution that the explanation for this shoulder comes from the consideration of the HH, HD, and DD bond length distribution in parent $NH_xD_{(5-x)}^{2+}$ and a portion of this distribution correlates with NX_3+X_2 products more significantly, which is shown in Figs. 4-6.

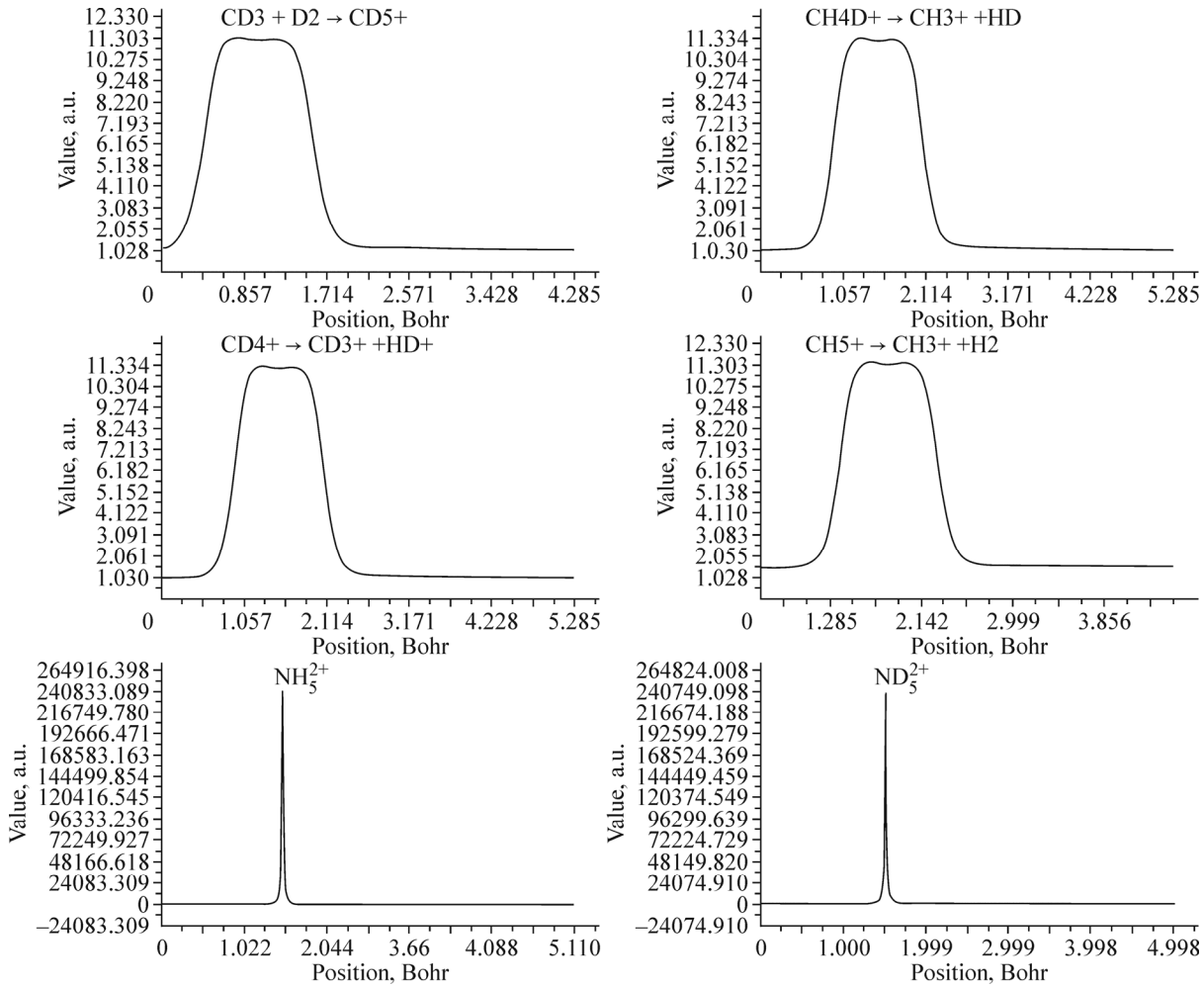

Fig. 6. Average local ionization energy for CH_5^+, CD_5^+, CH_4D^+, CHD_4^+ and Hamiltonian kinetic energy for $NH_xD_{(5-x)}^{2+}$ ($x = 0, 5$).

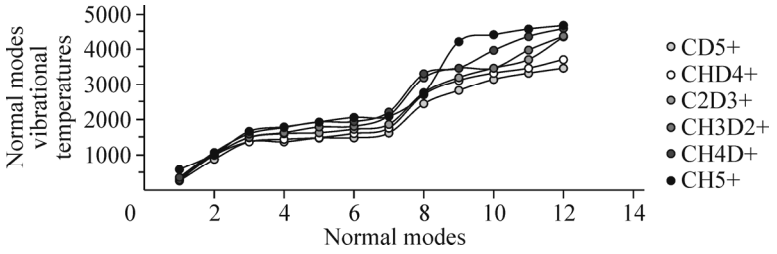

Fig. 7. Normal vibrational mode temperature for $CH_xD_{(5-x)}^+$ variants.

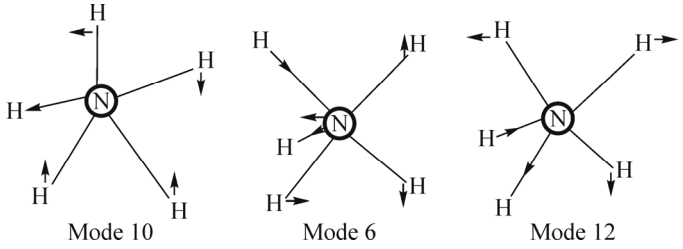

Fig. 8. Normal vibrational modes 6, 10, 12 of NH_5^{2+}.

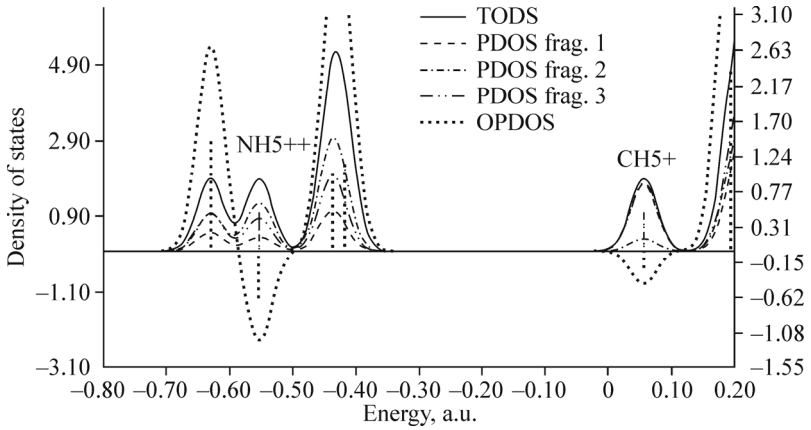

Fig. 9. Density of states, including a comparison of NH_5^{++} and CH_5^+.

Ivanov [18] and coworkers have shown that classical *ab initio* molecular dynamics indeed closely reproduces the binomial distributions expected for these site occupations while the full quantum simulations reveal the quantum populations strongly deviating from classical (binomial) occupations. Here, there is a point: is there any real or artefactual rotation in quantum approaches? In other words, there is a symmetry breaking among classical and quantum approaches only for X_2 as a part of the molecule. On partial D ↔ H substitutions, the scrambling phenomenon appeared in different isotopic nuclei for the population of all available sites, i.e., these in the X_2 moiety. The local information entropy data (Tables 1-4) and entropy (Table 6) indicate that $NH_xD_{(5-x)}^{2+}$ has binomial distributions but for two parts inside the molecule. Considering the ZPE differences of D and H, it might be indicated that deuterons prefer to populate the NX_3 tripod in the mixed isotopologues NH_4D^{2+} and NHD_4^{2+}, whereas protons in the X_2 moiety are compared to the purely combinatory probabilities.

Quantum mechanical fluctuations due to Boltzmann statistics cause systematic deviations of H and D sites from the underlying combinatorial symmetries, and thereby induce a breaking of this symmetry. LOL and ELF (Tables 1-4) have confirmed the approaches of quantum localization used in this work. This effect is relevant at all vibrational normal modes and, as can be seen, these intricate nuclear quantum effects are certain ways for understanding the experimental spectra [55].

The distribution correlating with NH_3^{2+} and H_2 exhibits a larger contribution with the shorter H–H distance than the longer one. In addition, the vibrational excited state of H–H with the larger hydrogen-hydrogen bond length indicates a greater contribution than that of the shorter one (in contrast to D–D), while for H–D it depends on the combinations of isotopologues.

Through the normal mode analysis, it can be seen that partial D ↔ H substitutions break the rotational symmetry.

CONCLUSIONS

The present results of normal modes 6, 10 and 12 qualitatively agree with NH_5^{++} which are highly fluxional and have a complex spectrum while the N–X bonds are broken and reformed all the time *via* quantum/classical distributions of two terms for X–X (X: H or D) and the remaining segment of these molecules. The spectrum of mode 10 is highly complex with huge red and some blue shifts. In particular, they can be attributed to the rapid coupling of the original NH stretching normal mode to motions more closely related to isomerization, i.e., bending or rocking. There has been a long debate whether NH_5^{2+} has a structure at all or not and whether it has real or artefactual rotation. It is supposed that only two N–X bonds in a part of molecules obey quantum populations while the remaining section of these molecules have the classical occupations which are an artefactual rotation in $NH_xD_{(5-x)}^{2+}$.

CONFLICT OF INTERESTS

The author declares that he has no conflict of interests.

REFERENCES

1. D. Marx and M. Parrinello. *Science*, **1999**, *284*, 59.
2. P. R. Schreiner. *Angew*. *Chem. Int. Ed.*, **2000**, *39*(18), 3239.
3. A. B. McCoy, B. J. Braams, A. Brown, Xinchuan Huang, Zhong Jin, and Joel M. Bowman. *J. Phys. Chem. A*, **2004**, *108*, 4991.
4. A. L. Kaledin, S. D. Kunikeev, and H. S. Taylor. *J. Phys. Chem. A*, **2004**, *108*, 4995.
5. A. Brown, B. J. Braams, K. Christoffel, Z. Jin, and J. M. Bowman. *J. Chem. Phys*., **2003**, *119*, 8790.
6. A. Brown, A. B. McCoy, B. J. Braams, Z. Jin, and J. M. Bowman. *J. Chem. Phys*., **2004**, *121*, 4105.
7. G. A. Olah and G. Rasul. *Acc. Chem. Res*., **1997**, *30*, 245–250.
8. G. A. Olah, G. K. S. Prakash, and J. Sommer. Superacids. Wiley and Sons: New York a.o., **1985**, *371*.
9. G. A. Olah, G. K. S. Prakash, R. E. Williams, L. D. Field, and K. Wade. Hypercarbon Chemistry. Wiley: New York, **1987**, 191–213.
10. T. Oka. *Trans. Roy. Soc. Lond. A*, **1988**, *324*, 81–95.
11. E. Herbst. *J. Phys. Chem. A*, **2005**, *109*, 4017–4029.
12. D. Gerlich. *Phys. Chem. Chem. Phys*., **2005**, *7*, 1583–1591.
13. K. C. Thompson, D. L. Crittenden, and M. J. T. Jordan. *J. Am. Chem. Soc*., **2005**, *127*, 4954–4958.
14. P. R. Schreiner, S.-J. Kim, H. F. Schaefer III, and P. von. R. Schleyer. *J. Chem. Phys*., **1993**, *99*, 3716.
15. V. Dyczmons and W. Kutzelnigg. *Theor. Chim. Acta* (*Berlin*), **1974**, *33*, 239–247.
16. H. Müller, W. Kutzelnigg, J. Noga, and W. Klopper. *J. Chem. Phys*., **1997**, *106*, 1863–1869.
17. D. Marx and M. Parrinello. *Nature*, **1995**, *375*, 216–218.
18. S. D. Ivanov, O. Asvany, A. Witt, E. Hugo, G. Mathias, B. Redlich, D. Marx, and S. Schlemmer. *Nature Chem.*, **2010**, 298–302.
19. S. Schlemmer, E. Lescop, J. von Richthofen, D. Gerlich, and M. A. Smith. *J. Chem. Phys*., **2002**, *117*, 2068–2075.
20. S. Schlemmer and O. Asvany. *J. Phys.: Conf*., **2005**, *4*, 134–141.
21. D. Marx and J. Hutter. *Ab initio* Molecular Dynamics: Basic Theory and Advanced Methods. Cambridge Univ. Press, **2009**.
22. A. J. R. Heck L. J. de Koning, and N. M. M. Nibbering. *J. Am. Soc*., *Mass. Spectrom*., **1991**, *2*, 453.
23. T. Lu and F. Chen. *Acta Chim. Sinica*, **2011**, *69*, 2393–2406.
24. T. Lu and F. Chen. *J. Mol. Graph. Model*, **2012**, *38*, 314–323.
25. T. Lu and F. Chen. *J. Comp. Chem*., **2012**, *33*, 580–592.
26. R. F. W. Bader. Atoms in Molecule: A Quantum Theory. Oxford Univ. Press: Oxford, **1990**.
27. A. D. Becke and K. E. Edgecombe. *J. Chem. Phys*., **1990**, *92*, 5397.
28. A. Savin et al. *Angew*. *Chem. Int. Ed. Engl*., **1992**, *31*, 187.
29. V. Tsirelson and A. Stash. *Chem. Phys. Lett*., **2002**, *351*, 142.
30. H. L. Schmider and A. D. Becke. *J. Mol. Struct. (THEOCHEM)*, *527*, 51.
31. C. Aslangul et al. *Adv. Quantum Chem*., **1972**, *6*, 93.
32. R. Parr et al. *J. Phys. Chem*. *A*, **2005**, *109*, 3957.
33. S. Noorizadeh and E. Shakerzadeh. *Phys. Chem. Chem. Phys*., **2010**, *12*, 4742.
34. J. S. Murray and P. Politzer. *J. Mol. Struct. (THEOCHEM)*, **1994**, *307*, 55.

35. M. W. Schmidt, K. K. Baldridge, J. A. Boatz, S. T. Elbert, M. S. Gordon, J. H. Jensen, S. Koseki, N. Matsunaga, K.A. Nguyen et al. *J. Comput. Chem*., **2004**, *14*(11), 1347–1363.
36. T. H. Dunning Jr. *J. Chem. Phys*., **1989**, *90*, 1007.
37. Y. Zhao and D. G. Truhlar. *Theor. Chem. Account*., **2008**, *120*, 215–241.
38. W. Kohn, L. J. Sham. *Phys. Rev*., **1965**, *140A*, 1133–1138.
39. J. P. Perdew, K. Burke, and M. Ernzerhof. *Phys. Rev. Lett*., **1996**, *77*, 3865–3868.
40. A. R. Ilkhani and M. Monajjemi. *Comput. Theor. Chem*., **2015**, *1074*, 19–25.
41. M. Monajjemi and J. E. Boggs. *J. Phys. Chem. A*, **2013**, *117*, 1670–1684, DOI: 10.1021/jp312073q.
42. M. Monajjemi, V. S. Lee, M. Khaleghian, B. Honarparvar, and F. Mollaamin. *J. Phys. Chem. C*, **2010**, *114* 15315, DOI: 10.1021/jp104274z.
43. M. Monajjemi. *J. Mol. Modeling*, **2014**, *20*, 2507, DOI: 10.1007/s00894-014-2507-y.
44. M. Monajjemi. *Theor. Chem. Acc*., **2015**, *134*, 77, DOI 10.1007/s00214-015-1668-9.
45. M. Monajjemi. *Struct. Chem*., **2012**, *23*, 551, DOI: 10.1007/s11224-011-9895-8.
46. M. Monajjemi. *Chem. Phys*., **2013**, *425*, 29–45, DOI: 10.1016/j.chemphys.2013.07.014.
47. H. Jalilian and M. Monajjemi. *Jpn. J. Appl. Phys*., **2015**, *54*, 085101, DOI: 10.7567/JJAP.54.085101.
48. M. Monajjemi and M. Khaleghian. *J. Cluster Sci*., **2011**, *22*(4), 673–692, DOI: 10.1007/s10876-011-0414-2.
49. M. Monajjemi, M. Falahati, and F. Mollaamin. *Ionics*, **2013**, *19*(1), 155–164, DOI: 10.1007/s11581-012-0708-x.
50. M. Monajjemi. *Biophys. Chem*., **2015**, *207*, 114–127, DOI: 10.1016/j.bpc.2015.10.003.
51. L. Mahdavian and M. Monajjemi. *Microelectron. J*., **2010**, *41*(2-3), 142–149, DOI: 10.1016/j.mejo.2010.01.011.
52. M. Monajjemi. *J. Mol. Liquids*, **2017**, *230*, 461–472, DOI: 10.1016/j.mejo.2010.01.011.
53. M. Monajjemi. *Macedonian J. Chem.*, *Chem. Engineering*, **2017**, *36*(1), 101–118.
54. H. Jacobsen. *Can. J. Chem*., **2008**, *86*(7)*,* 695–702, https://doi.org/10.1139/v08-052.
55. E. Herbst. *J. Phys. Chem. A*, **2005**, *109*, 4017–4029.